Clinical mutations in WDR34 lead to diverse impacts on the assembly and function of dynein-2

Caroline Shak[1], Laura Vuolo[1], Borhan Uddin[1,4], Yohei Katoh[3], Tom Brown[1], Kate Heesom[2], Nicola Stevenson[1], Kazuhisa Nakayama[3], David J. Stephens[1]*

[1] Cell Biology Laboratories, School of Biochemistry, Faculty of Life Sciences, University of Bristol, Bristol BS8 1TD, UK; [2] Proteomics Facility, Faculty of Life Sciences, University of Bristol, BS8 1TD, UK; [3] Department of Physiological Chemistry, Graduate School of Pharmaceutical Sciences, Kyoto University, Sakyo-ku, Kyoto 606-8501, Japan; [4] Present address: Department of Biochemistry and Molecular Biology, Jahangirnagar University Dhaka, Bangladesh.

* corresponding author: david.stephens@bristol.ac.uk

Open Researcher and Contributor IDs (ORCID)

David Stephens	0000-0001-5297-3240
Caroline Shak	0000-0002-2109-1058
Borhan Uddin	0000-0001-9142-7568
Laura Vuolo	0000-0002-9801-9206
Nicola Stevenson	0000-0001-8967-7277
Yohei Katoh	0000-0003-1649-4917
Kazuhisa Nakayama	0000-0001-7701-7183

Running title: Impact of clinical mutations in WDR34

Keywords: Cilia, dynein-2, microtubule motors, intraflagellar transport

Summary statement

Clinical mutations in WDR34 are found to have diverse impacts on ciliogenesis and cilia function following stable expression in a WDR34 knockout cell model.

Abstract

The primary cilium is a sensory organelle, receiving signals from the external environment and relaying them into the cell. Mutations in proteins required for transport in the primary cilium result in ciliopathies, a group of genetic disorders that commonly lead to the malformation of organs such as the kidney, liver and eyes and skeletal deformation. Motor proteins dynein-2 and kinesin-2 mediate retrograde and anterograde transport in the cilium. WDR34, a dynein-2 intermediate chain, is required for the maintenance of cilia function. Here, we investigated WDR34 mutations identified in Jeune syndrome, Short-rib polydactyly syndrome or Asphyxiating thoracic dysplasia patients by stably expressing the mutant proteins in WDR34 knockout cells. WDR34 mutations led to different spectrums of phenotypes. Each mutation results in a distinct profile of phenotypes. Quantitative proteomics demonstrated changes in dynein-2 assembly, whereas initiation and extension of the axoneme, IFT-B protein localization, transition zone integrity, and Hedgehog signalling were also affected.

Introduction

The primary cilium is a microtubule-based structure that protrudes from the cell surface, its membrane continuous with the plasma membrane. The organelle acts as a cellular antenna, detecting stimuli from the surrounding environment and transmitting the information into the cell via receptors on its surface to mediate the appropriate response. Primary cilia have a major role in Hedgehog (Hh) signalling , directing proliferation, migration, and differentiation of cells with a particular importance during skeletal development (Goetz and Anderson, 2010). Defects in cilia assembly and function lead to a wide range of ciliopathies (Reiter and Leroux, 2017).

Assembly and ongoing function of the primary cilium is mediated by intraflagellar transport (IFT) of cargoes (Kozminski et al., 1993; Pigino, 2021; Webb et al., 2020). IFT is bidirectional and utilizes organelle specific motors kinesin-2 and cytoplasmic dynein-2 (hereafter referred to as dynein-2) to transit along microtubules doublets arranged along the central axis of the cilium (Pigino, 2021; Vuolo et al., 2020). Kinesin-2 works with IFT-B trains (Funabashi et al., 2018) to drive anterograde transport of cargoes along B-tubules of the microtubule doublets (Stepanek and Pigino, 2016) towards the tip of the cilium. Anterograde IFT trains also include IFT-A proteins and inactive dynein-2 (Jordan et al., 2018; Toropova et al., 2017; Toropova et al., 2019; Webb et al., 2020). At the tip, and likely at other sites along the axoneme (Nievergelt et al., 2021), reassembly of proteins and a change in conformation of dynein-2 leads to its activation, allowing retrograde trafficking of proteins by dynein-2 and IFT-A trains along the A-tubules of the microtubule doublets (Stepanek and Pigino, 2016). A ciliary necklace (Gilula and Satir, 1972) connects to the transition zone (TZ), distal to the mother centriole, to form a diffusion barrier at the ciliary base from which proteins enter and exit the organelle. IFT is required both to maintain the transition zone (Jensen et al., 2018; Vuolo et al., 2018) as well as enable crossing of this barrier (De-Castro et al., 2022; Park and Leroux, 2022).

Metazoan dynein-2 is formed of multiple subunits (Asante et al., 2014; Vuolo et al., 2020) built around two copies of the dynein heavy chains ((encoded by DYNC2H1) (Pazour et al., 1999; Porter et al., 1999; Signor et al., 1999)). The motor complex is asymmetric, containing two different dynein-2 intermediate chains (Asante et al., 2014; Toropova et al., 2019): DYNC2I1 (originally identified as FAP163 in *Chlamydomonas* (Patel-King et al., 2013) and commonly called WDR60 in mammals) and DYNC2I2 (originally identified as FAP133 in *Chlamydomonas* (Rompolas et al., 2007) and commonly called WDR34 in mammals). They each contain N-terminal regions that bind dynein light chains (Pazour et al., 1998) and a C-terminal WD-propellor structure, each of which binds one dynein-2 heavy chain (Toropova et al., 2019). A dimeric dynein-2-specific light intermediate chain, commonly called LIC3 (encoded by DYNC2LI1 (Grissom et al., 2002; Hou et al., 2004)), in turn binds to and stabilizes the individual heavy chains. Light chains encoded by DYNLL1 and DYNLL2 (LC8 family), DYNLRB1 and DYNLRB2 (roadblock family), DYNLT1 and DYNLT2 (Tctex family) are shared with dynein-1; DYNLT2B encoding TCTEX1D2 is unique to dynein-2 (Asante et al., 2014). We use the more common names throughout for ease of reading.

Mutations in each of the genes encoding dynein-2 subunits lead to ciliopathies, specifically, those associated with skeletal abnormalities (Huber and Cormier-Daire, 2012). In particular, multiple studies have identified WDR34 mutations in individuals with Jeune syndrome or Short-rib polydactyly syndrome (SRPS) (Huber et al., 2013; Schmidts et al., 2013; You et al., 2017) with more continuing to be identified (Yin et al., 2020). Clinical phenotypes differ between individuals (Schmidts et al., 2013). The homozygous missense mutation c.65C>T (A22V) was identified with homozygous DYNC2H1 and heterozygous mutations in IFT140 c.4058C>G in an individual who died in infancy. The heterozygous missense mutation c.443G>T (C148F) was identified in an individual with a protruding abdomen and hepatic ptosis and died aged 46 days. The heterozygous

nonsense mutation c.472C>T (Q158*) was reported with heterozygous missense c.1307A>G (K436R) in an eight year old with rod-cone dystrophy, obesity, and speech and language delay. The missense homozygous c.616C>T (R206C) was reported in an eight year old with polydactyly. The missense homozygous c.1169C>T (P390L) mutation was identified with heterozygous WDR19 c.2720C>T in an individual with bilateral nephrocalcinosis who died at an unreported age. The missense c.1177G>A (G393S) mutation was identified four times from two unrelated families. Two individuals from the first family shared a homozygous mutation leading to death of one individual at 4 months and the other at an unspecified age. The mutation was also identified as a heterozygous mutation with heterozygous c.1541_1542delCA (T514Afs*11) in two prenatal testing from the second family, with neither pregnancies reaching term. The homozygous missense mutation c.1229G>T (S410I) was reported in an 8.5 year old individual with vision impairment. The missense homozygous c.1339C>T (R447W) was identified in two individuals from the same family, one dying immediately after birth, and one born at 34 weeks gestation with elevated cerebrospinal fluid spaces, foot malformation, umbilical hernia and dying after 2 days.

WDR34 mutations were also identified in individuals with SRPS or asphyxiating thoracic dysplasia (ATD) (Huber et al., 2013). The homozygous missense mutation c.1022C>T (A341V) was identified three times in the same family, one case was terminated during pregnancy, one case was stillborn due to hypertrophic lungs, and one case died at seven days of age. The homozygous missense mutation c.1061C>T (T354M) was identified in one individual who was carried to term. The homozygous missense mutation c. 1339C>T (R447W), also identified in Schmidts et al., (2013) was identified in a case with polydactyly and was terminated during pregnancy. Compound heterozygous missense mutations c.1340G>A (R447Q) and c.982-2T>G was identified in a case that was terminated during pregnancy. Another study identified the homozygous missense mutation c.544C>T (R182W) in an individual with SRPS including polydactyly, lung and pulmonary problems who died at four months of age (You et al., 2017). WDR34-T514Afs*11 is not included in this study.

Although these mutations are often homozygous, they are not always found in isolation (Schmidts et al., 2013). It has been suggested that mutations could act in trans and digenic inheritance has been proposed in some cases, complicating the explanation of clinical presentations. For example, patients with WDR34-A22V mutations were also heterozygous for other mutations in WDR19 and IFT140 that are predicted to be deleterious to function (Schmidts et al., 2013).

Knockout (KO) models of WDR34 have been studied in cells and model organisms (Huber et al., 2013; Schmidts et al., 2013; Wu et al., 2017). A WDR34 KO cell culture model containing only the first 24 or 44 residues of WDR34 resulted in longer cilia, mis-localization of the IFT-B protein IFT88 and impaired Hh signalling (Tsurumi et al., 2019). Similar but more pronounced phenotypes were observed in WDR60 KO cells (Hamada et al., 2018; Tsurumi et al., 2019, Vuolo et al., 2018). Different WDR34 KO cell lines (Tsurumi et al., 2019; Vuolo et al., 2018) and a KO mouse model (Wu et al., 2017) have been reported to have very short primary cilia; notably these retain expression of a longer N-terminal WDR34 region of 114-146 amino acids. These KO models, show changes in IFT88 and IFT140 distribution (Vuolo et al., 2018; Wu et al., 2017), impaired Hh signalling (Wu et al., 2017), and reduced assembly of the dynein-2 holocomplex (Vuolo et al., 2018). It has been proposed that ongoing expression of the truncated WDR34 protein in these cells results in a dominant negative phenotype (Tsurumi et al., 2019). Indeed, this may also be a major impact of the clinical WDR34 Q158* mutation (Huber et al., 2013).

In this study we set out to determine the impact solely of the mutations in WDR34 to gain a better understanding of the disease phenotypes as well as the role of this key dynein-2 subunit. Here, we have examined the ability of clinically identified point mutations in WDR34 to restore normal ciliary

structure and function to WDR34 KO cells. Using proteomics, biochemistry, and cell imaging, our data show that WDR34 mutations have diverse impacts on dynein-2 integrity, ciliogenesis, cilia length control, and signalling . Notably, many mutations can restore significant aspects of cilia function and selective defects are seen with each mutation.

Results

Twelve point mutations and one truncation mutation in WDR34 were investigated (Fig. 1A). Eleven of the residues are well conserved amongst species (summarized in Supplementary Figure S1), suggesting a significant role in protein function.

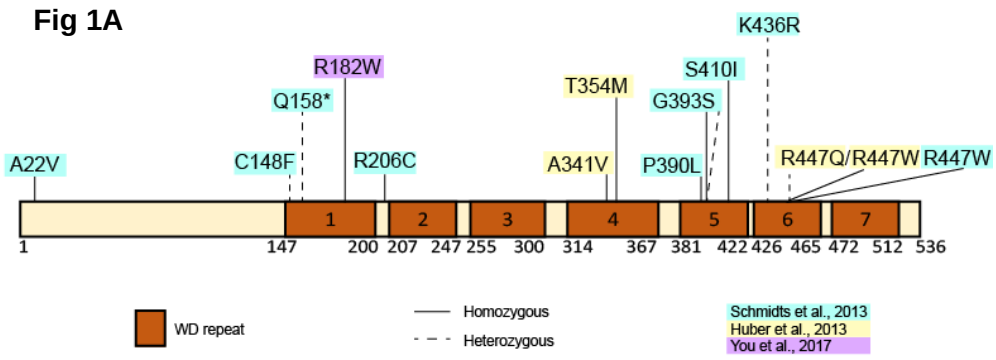

Figure 1A WDR34 mutations in patients. (A) Whole exome screening identified 15 point mutations located throughout the length of the protein. The 14 investigated in this study are shown, 13 missense mutations and one resulting in a premature stop codon.

The location of each mutant relative to its position within the dynein-2 complex is shown in Supplementary Figure S2. To study these WDR34 mutations, we used retinal pigment epithelial (RPE1) cells engineered using CRISPR to knockout expression of WDR34 (Tsurumi et al., 2019) and transduced them with lentiviruses to stably express wild-type (WT) GFP-WDR34, specific WDR34 mutants, or GFP only. All constructs were expressed as intact proteins at the expected molecular weight, as shown by immunoblotting of cell lysates, but at different levels, as indicated by band intensities (Fig. 1B). Notably, GFP-WDR34-Q158* was expressed at a low level. Throughout this study, the cell lines were serum starved to stimulate ciliogenesis, allowing the investigation of cilia defects.

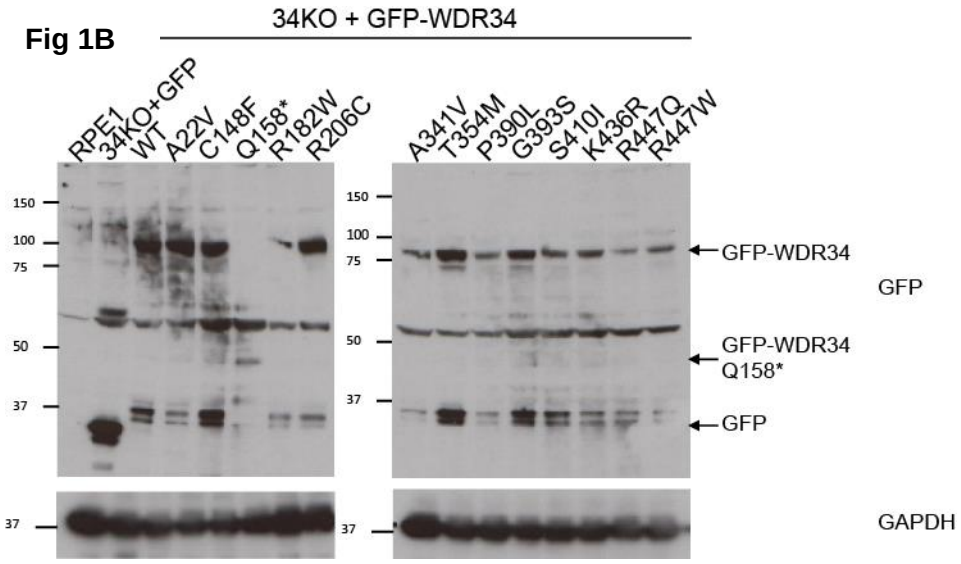

Figure 1B Expression of GFP-WDR34 mutants was confirmed by immunoblotting using an anti-GFP antibody with GAPDH as a loading control. Molecular weights are shown in kDa. Note that all lanes show a non-specific band at ~60 kDa.

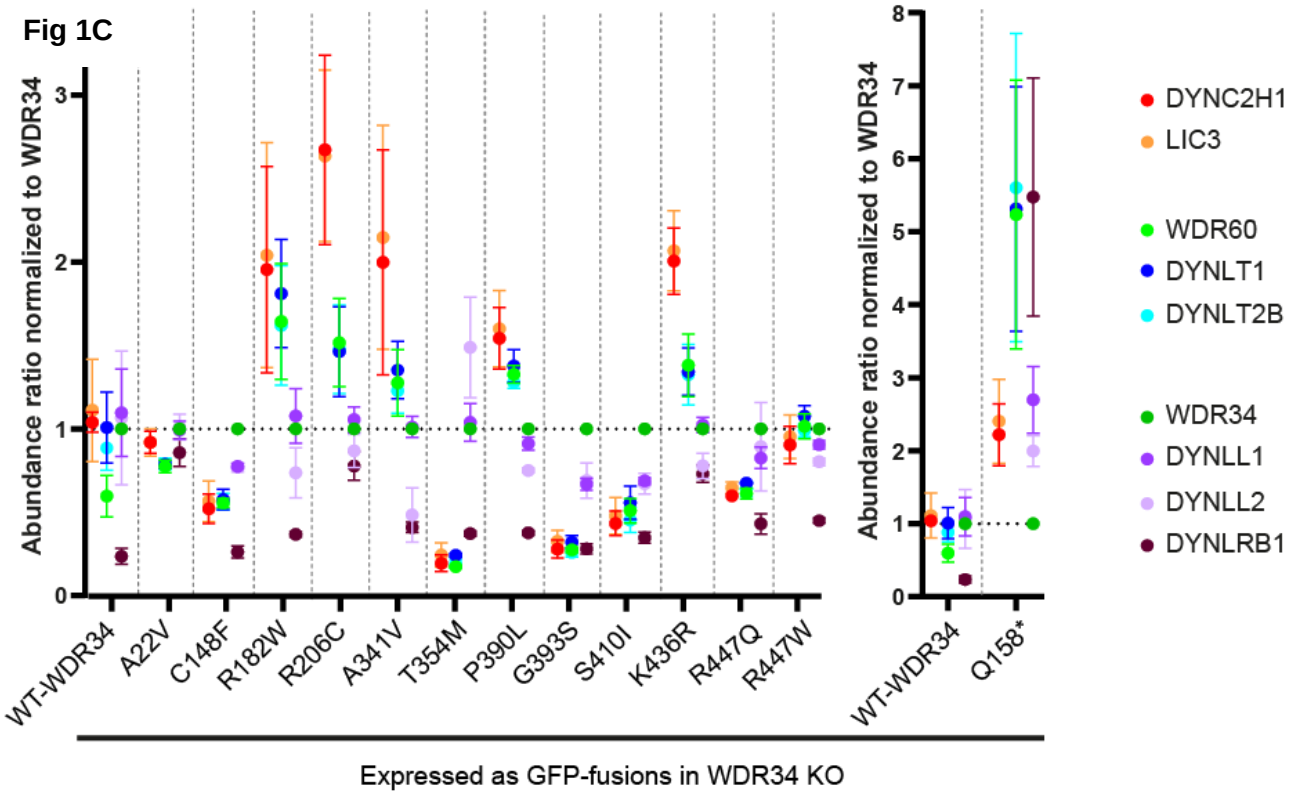

Figure 1C WDR34 mutants interact differently with DYNC2H1-LIC3 and WDR60-DYNLT2B-DYNLT1 subcomplexes, and DYNLRB1. RPE1 WDR34 KO cell lines expressing GFP proteins were serum-starved for 24 h to induce ciliogenesis and harvested to purify GFP proteins by GFP-trap. Proteomics of GFP-WDR34 proteins by TMT-labelling was used to relatively quantify interaction with other dynein-2 proteins. Protein abundances were normalized to WDR34. (D) Separate plot for GFP-WDR34-Q158* plotted along with GFP-WDR34 WT (as in C) owing to different scaling of the y-axis.

Impact of WDR34 mutations on dynein-2 complex assembly

We utilized 16-plex multiplex tandem-mass-tag (TMT)-labelling to relatively quantify the interaction of WDR34 point mutant proteins with other dynein-2 components. To prepare cell samples for proteomics, clarified protein lysates were incubated with GFP-Trap beads to identify proteins interacting with GFP-WDR34. Purified proteins were labelled with tandem labelled tags prior to MS analysis to allow the relative quantification of proteins in each sample. Each sample was normalized relative to the abundance of WDR34 to account for differences in expression level and protein stability. Dynein-2 complex components DYNC2H1, WDR60, LIC3, DYNLL1, DYNLL2, DYNLRB1, DYNLT1 and DYNLT2B were identified as interacting partners across all samples in all three experimental repeats (Fig. 1C, D). DYNLRB2 and DYNLT3 were not identified in these experiments.

Dynein-2 can be split into three subcomplexes (Hamada et al., 2018), DYNC2H1-LIC3, WDR60-TCTEX1D2-DYNLT1, and WDR34-DYNLL1/DYNLL2-DYNLRB1. Association of WDR34 A22V, R447Q and R447W with DYNC2H1-LIC3 and WDR60-TCTEX1D2-DYNLT1 was similar to WDR34 WT. Mutations that resulted in a >50% reduction in interaction were C148F, T354M, G393S and S410I, whereas mutations that resulted in a 2-fold increased interaction with DYNC2H1-LIC3 were Q158*, R182W, R206C, A341V and K436R. These WDR34 mutants also resulted in a modestly increased interaction with WDR60-DYNLT2B-DYNLT1 (Fig. 1C).

Formation of the third dynein-2 subcomplex, WDR34-DYNLL1/DYNLL2-DYNLRB1 involves binding of the light chains to the N-terminal region of WDR34 (Toropova et al., 2019). Interestingly, apart

from WDR34-K436R, interaction with DYNLRB1 was reduced by more than half in all WDR34 point mutants located in a WD domain, suggesting defective assembly of DYNLRB1 in dynein-2 may be a common phenotype in WDR34-related disorders. The association of DYNLL2 with WDR34 was only significantly reduced in cells expressing WDR34-A341V, whereas DYNLL1 was not markedly affected. The differences in light chain binding to WDR34 mutants suggest they bind independent of one another. These results show that WDR34 mutations impact dynein-2 assembly by either enhancing or decreasing association depending on the mutation. These data are summarized graphically in Supplementary Figure S3.

Impact on ciliogenesis and cilia length

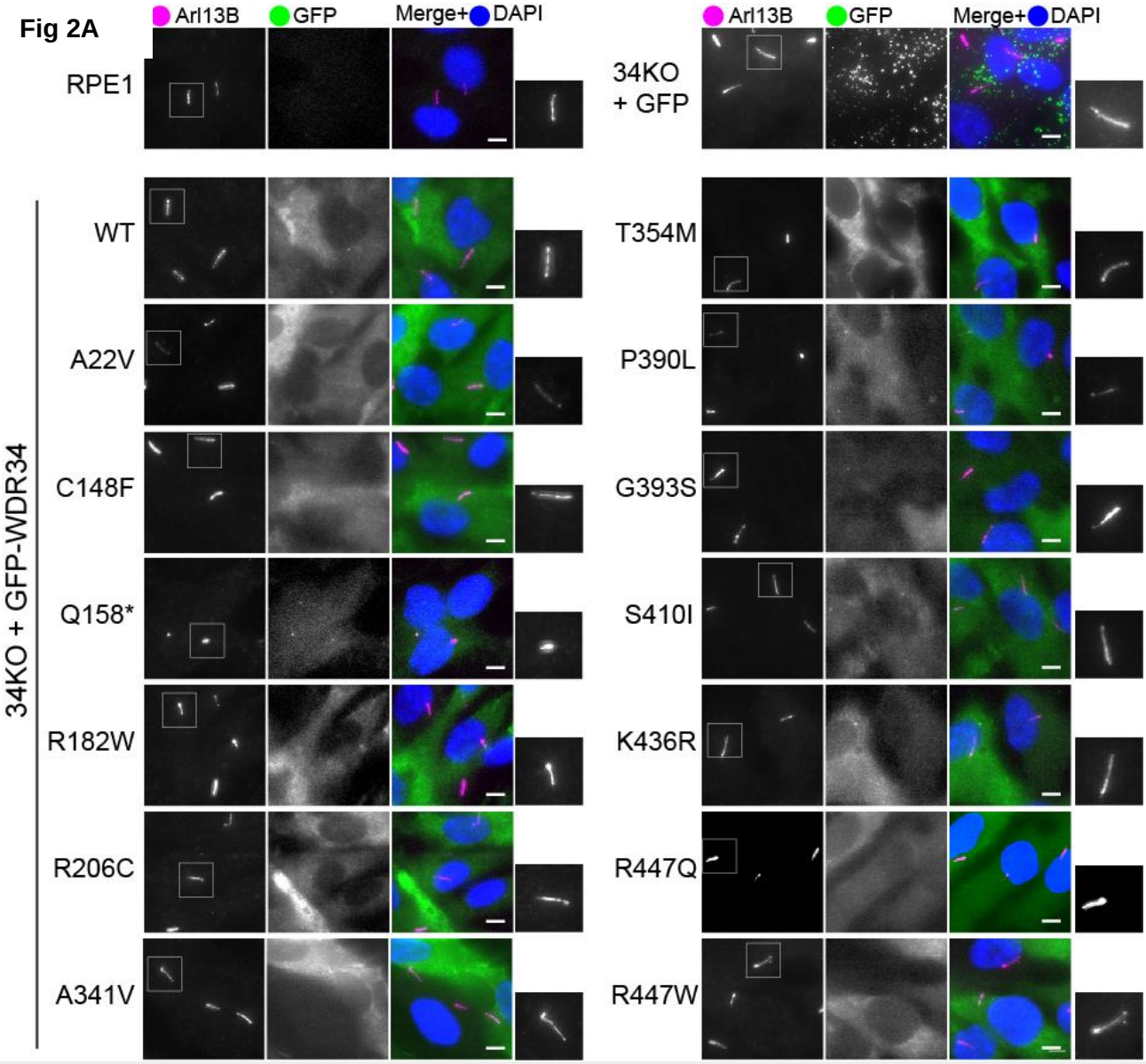

Figure 2A Formation and length of cilia is affected by WDR34 mutations. (A) WT RPE1 and WDR34 KO cell lines expressing GFP proteins (green) were serum-starved for 24 h to induce ciliogenesis and labelled to detect Arl13b (magenta). Scale bar = 5 µm. Two-fold enlargements of cilia staining are shown.

All GFP-WDR34 proteins showed a significant cytosolic pool (Fig. 2A) with some minor localization to centrioles. Consistent with immunoblotting, GFP-WDR34-Q158* was expressed at a lower level and was more prominently observed at the ciliary base. To examine the effect of WDR34 mutations on the regulation of ciliogenesis, cells were immunolabelled to detect the cilia membrane marker Arl13b (Fig. 2A). We scored the percentage of ciliated cells and cilia length, testing all cell

lines against the parental WDR34 KO expressing GFP only, experiments included WT RPE1 cells for comparison.

WDR34 KO cells have longer cilia than the WT RPE1 line as does the same control cell line used here expressing GFP (Fig. 2A, quantified in 2B), (Tsurumi et al., 2019). This contrasts with our own previous work (Vuolo et al., 2018). This may be explained because the cell line from Vuolo et al (2018) still encodes a significant N-terminal region of WDR34 which could act in dominant negative fashion. The cell line used in this study (Tsurumi et al., 2019) has a Val24Alafs*74 mutation in WDR34 which presents a more complete knockout. Increased cilia length in these cells is consistent with a role for WDR34 in retrograde IFT.

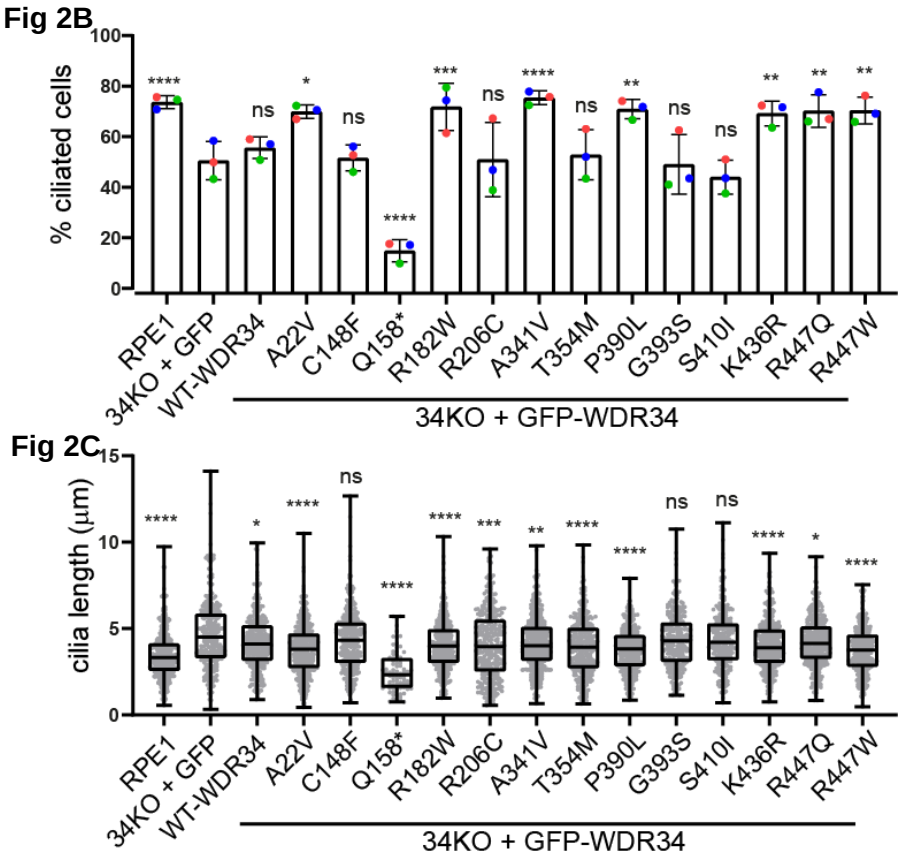

Figure 2B, C Percentage of ciliated cells in each cell line. Data pooled from three independent experiments with between 455 and 677 cells quantified. Data show means and standard deviation, n=3. *P=<0.05 using Tukey's multiple comparisons test. (C) Cilium length in each cell line. Data pooled from three independent experiments with between 78 and 406 cilia quantified. Box and whisker plot shows the median, interquartile ranges, minimum and maximum values, n=3. *P=<0.05 using Tukey's multiple comparisons test.

Expression of some mutants in the WDR34 KO line (A22V, R182W, A341V, P390L, K436R, R447Q, and R447W) led to an increase in the percentage of ciliated cells. The truncated version, Q158*, however, led to a significant reduction in the ability of cells to form cilia, consistent with a dominant negative impact on ciliogenesis (Tsurumi et al., 2019). The increase in cilia length in WDR34 KO cells is reversed in cells expressing WT WDR34 and almost all mutant proteins. The C148F, G393S and S410I mutations were not able to rescue cilia length. The Q158* mutation led to further reduction in cilia length, again suggesting the fragment acquired functions that are restrictive to cilia assembly (Tsurumi et al., 2019).

To summarize the proteomics and Arl13b data, WDR34 mutants that significantly increase the proportion of ciliated cells either showed no change or enhanced dynein-2 assembly. Conversely, mutations unable to rescue cilia length also showed reduced dynein-2 assembly.

Impact on the localization of RPGRIP1L

The transition zone (TZ) at the ciliary base mediates the entry and exit of proteins from the cilium. This diffusion barrier has been found to be disrupted in WDR60 KO cells (Vuolo et al., 2018). We

immunolabelled ciliated cells with an antibody against RPGRIP1L, a transition zone protein, to investigate whether this defect also arises in WDR34 KO cells and if so whether it could be "rescued" by any of the clinical mutations in WDR34 (Fig. 3A). As expected in RPE1 WT cells, RPGRIP1L was localized at the ciliary base as compact circular dots, adjacent to the basal body. In the WDR34KO-GFP cells, a proportion of the cells had RPGRIP1L staining which stretched and extended towards the cilium, similar to WDR60 KO cells (Vuolo et al., 2018). This was significantly reduced upon expression of WT WDR34. Apart from WDR34-R447Q, RPGRIP1L localization was similarly rescued by nearly all mutations, including the Q158* truncation (Fig. 3B), the only exception being the R447Q mutant. This supports a role for WDR34 in maintaining TZ integrity. Notably, of R447Q and R447W, only R447Q fails to restore the localization of RPGRIP1L. Our proteomics study showed that the interaction of WDR34-R447Q, but not R447W, with other dynein-2 proteins is slightly decreased.

Fig 3A

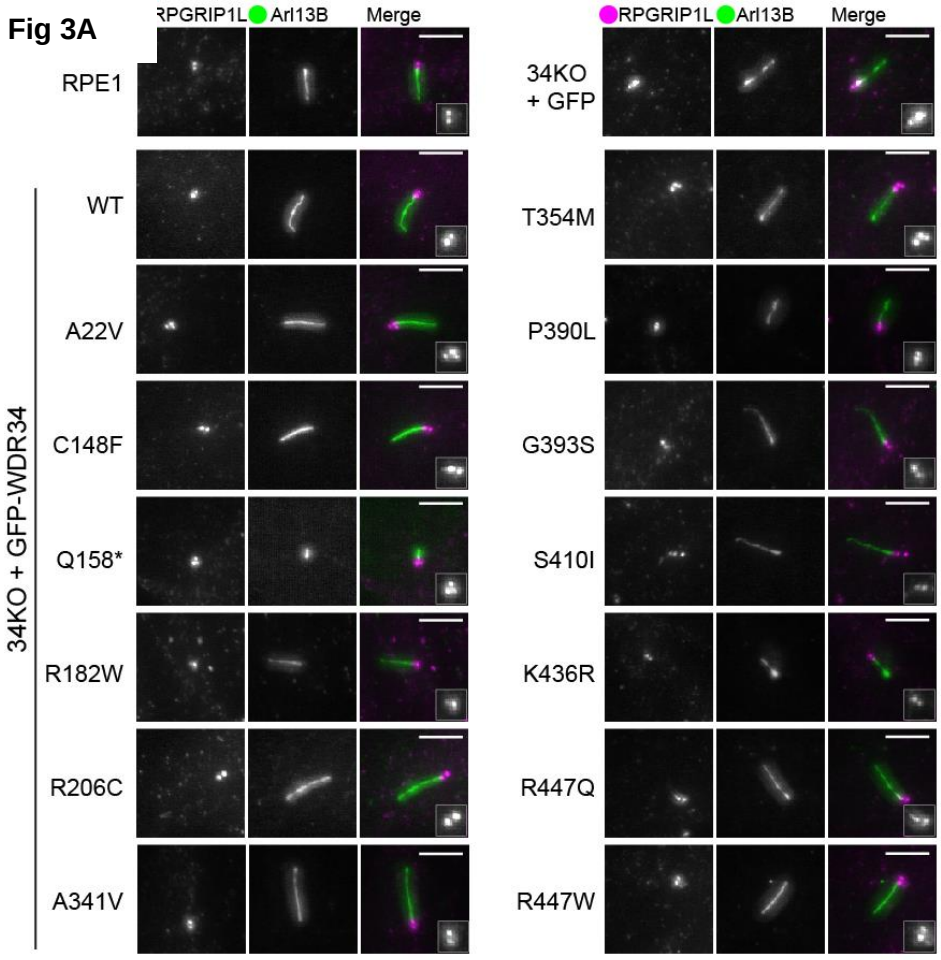

Fig 3B

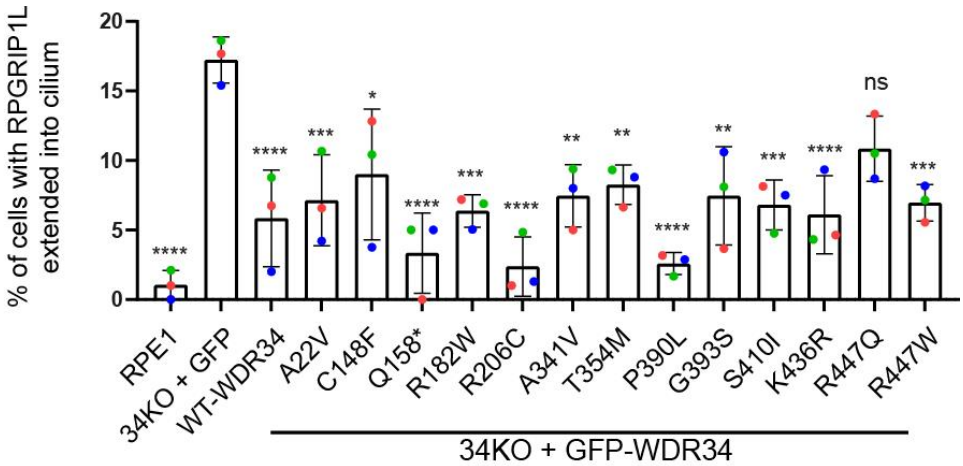

Figure 3 RPGRIP1L localization is only affected by WDR34-R447Q. (A) WT RPE1 and WDR34 KO cell lines expressing GFP proteins were serum-starved for 24 h to induce ciliogenesis and labelled with antibodies to detect Arl13b (green) and RPGRIP1L (magenta). Scale bar = 5 µm. 1.5-fold enlargements of RPGRIP1L staining are shown. (B) Percentage of cells with RPGRIP1L extension into the cilia. Between 95 and 455 cilia quantified in each case. Data show means and standard deviation, n=3 independent experiments. *P=<0.05 using Tukey's multiple comparisons test.

IFT140 localization

To analyse the effects of the WDR34 mutations on IFT-A proteins, IFT140 was immunolabelled alongside Arl13b as a ciliary marker (Fig. 4). In WDR34 KO cells, IFT140 localizes to the ciliary base, as it does in WT RPE-1 cells. The specific lot of IFT140 antibody used also stains non-specific nuclear dots, as observed by others (Hamada et al., 2018; Hirano et al., 2017; Takahara et al., 2019), and described by the manufacturer. This complicates analysis and so we have not quantified these data but instead scored for the robust presence of IFT140 by eye. Specific IFT140 staining was observed at the ciliary base in WDR34 KO cells expressing GFP only and nearly all WDR34 point mutations. This shows that WDR34 KO cells retain sufficient retrograde IFT function to maintain IFT140, and by inference the IFT-A complex, at the base. The only exception to this is seen with Q158* cells where IFT140 was seen throughout the length of the cilium, again suggesting that this truncated WDR34 protein results in dominant negative functions within the cilium, here in the assembly or localization of IFT-A.

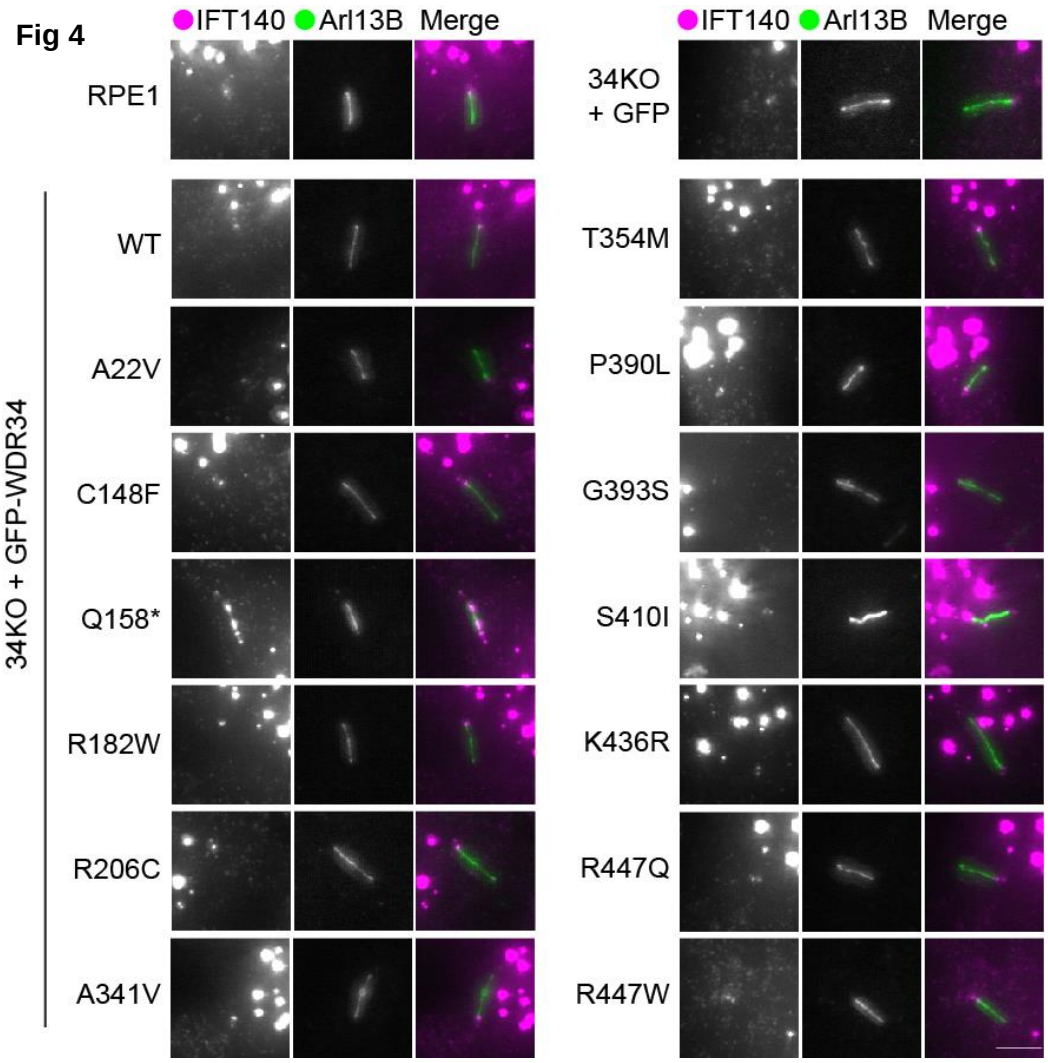

Figure 4 IFT140 missense is not affected by WDR34 missense mutations. WT RPE1 and WDR34 KO cell lines expressing GFP proteins were serum-starved for 24 h to induce ciliogenesis and stained with Arl13b and IFT140 antibodies. Bar = 5 µm.

Accumulation of IFT88 within the cilium

We next investigated the localization of the IFT-B protein, IFT88, as a well-characterized reporter of IFT defects. IFT88 is localized at the ciliary base in wildtype cells, but at the tips in WDR60 and WDR34 KO cells (Vuolo et al., 2018). We classified the distribution of IFT88 (Fig. 5A) into groups: base only, base and tip, throughout, and uniformly throughout (Fig. 5B). In RPE1 cells, IFT88 was mostly observed at the ciliary base and tip, or at the base only. In WDR34KO-GFP cells, the “base and throughout” localization became the most dominant distribution, whereas WDR34 WT rescued IFT88 distribution from the cilium length. The Q158* truncation results in a uniform distribution of IFT88 throughout the cilia. Only WDR34-A341V and T354M expressing cells also had an increased proportion of cilia with IFT88 along the cilium.

This change is concurrent with both a decrease in proportion of cells with IFT88 at the base only or base and tip, suggesting both localizations reflect normal IFT-B function.

Basal levels and SAG-stimulated localization of Smoothened in the cilium

The studies shown above provide insight to the assembly of the dynein-2 and IFT complexes. It is, however, the functional changes resulting from defects in IFT, such as trafficking of receptors and signalling proteins, that translate these mutations into disease phenotypes. Since WDR34 mutations lead to skeletal ciliopathies, Hh signalling is of key interest owing to its well-established roles in skeletal development. In cell culture, Hh signalling can be artificially stimulated with smoothened agonist (SAG). Under basal conditions, the GPCR family member smoothened (Smo) is typically excluded from cilia at the basal state and SAG stimulation promotes its entry into and accumulation within cilia.

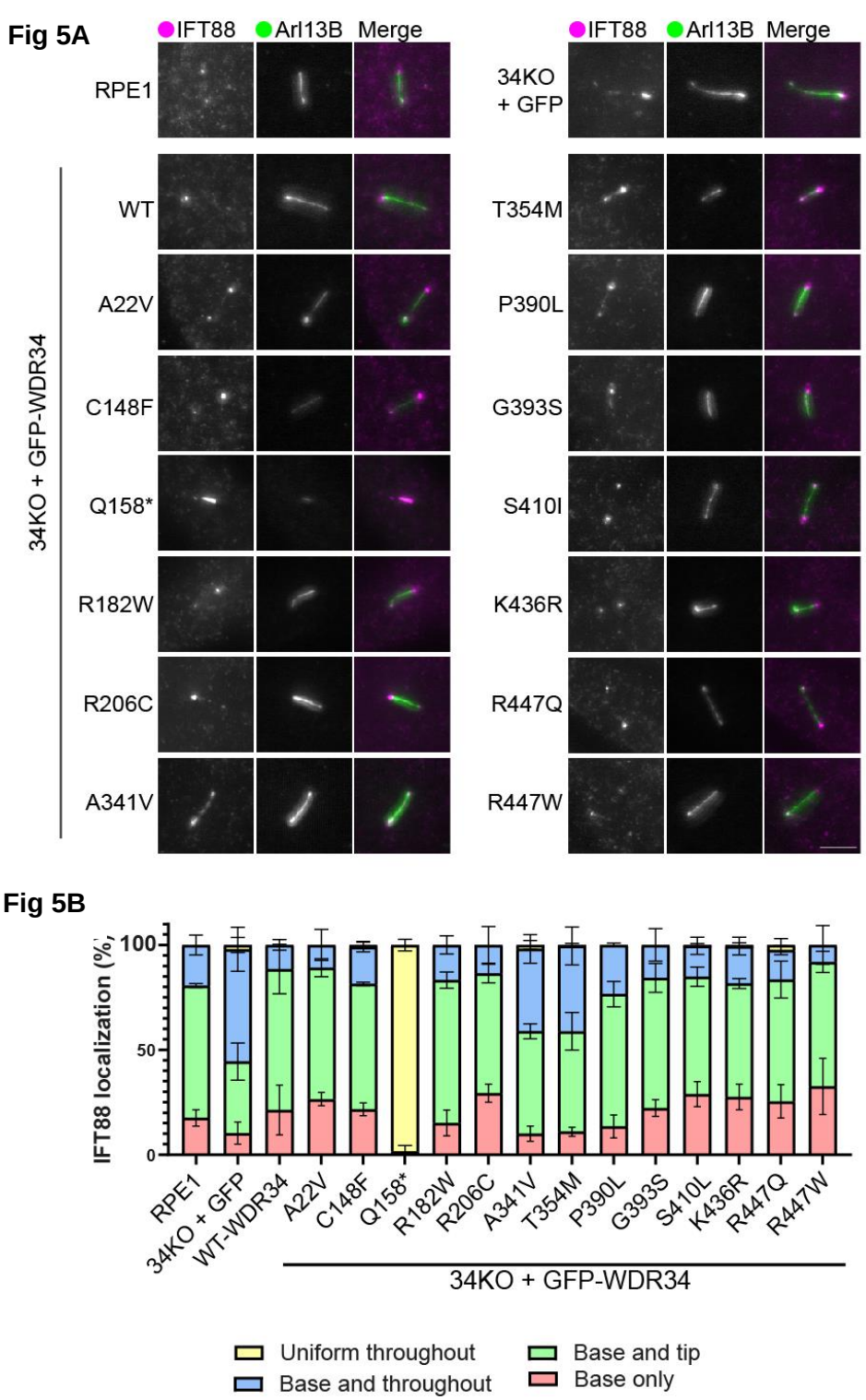

Figure 5 IFT188 localization is only affected by WDR34-A341V and WDR34-T354M. (A) WT RPE1 and WDR34 KO cell lines expressing GFP proteins were serum-starved for 24 h to induce ciliogenesis and stained with Arl13b (green) and IFT88 (magenta) antibodies. Scale bar = 5 µm. (B) Percentage of cells with various IFT88 distribution in each cell line. Cells were scored for IFT88 localization at the base only, throughout the cilium only, at the base and tip but not throughout the cilium, or at both base and cilia. Between 102 and 433 cilia quantified. Mean and standard deviation shown.

As expected in basal conditions, Smo is only observed in the cilium of a few cells in RPE1 WT cells (Fig. 6A). As shown previously for the cognate dynein-2 intermediate chain, WDR60 (Vuolo et al., 2018), WDR34 KO cells show Smo localization to the cilium under basal conditions in a greater proportion of cells (Fig. 6A, quantified in 6B). Expression of GFP-WDR34-WT was able to reduce basal levels of intra-ciliary Smo, albeit not to the same low level as RPE1 WT cells. Some WDR34 mutations could also restore this basal localization (C148F, R206C, T354M, P390L, and R447W) but A22V, R182W, A341V, G393S, S410I, K436R and R447Q could not. WDR34-K436R and Q158* showed more severe defects where basal Smo levels were greater than in the absence of WDR34.

Fig 6A

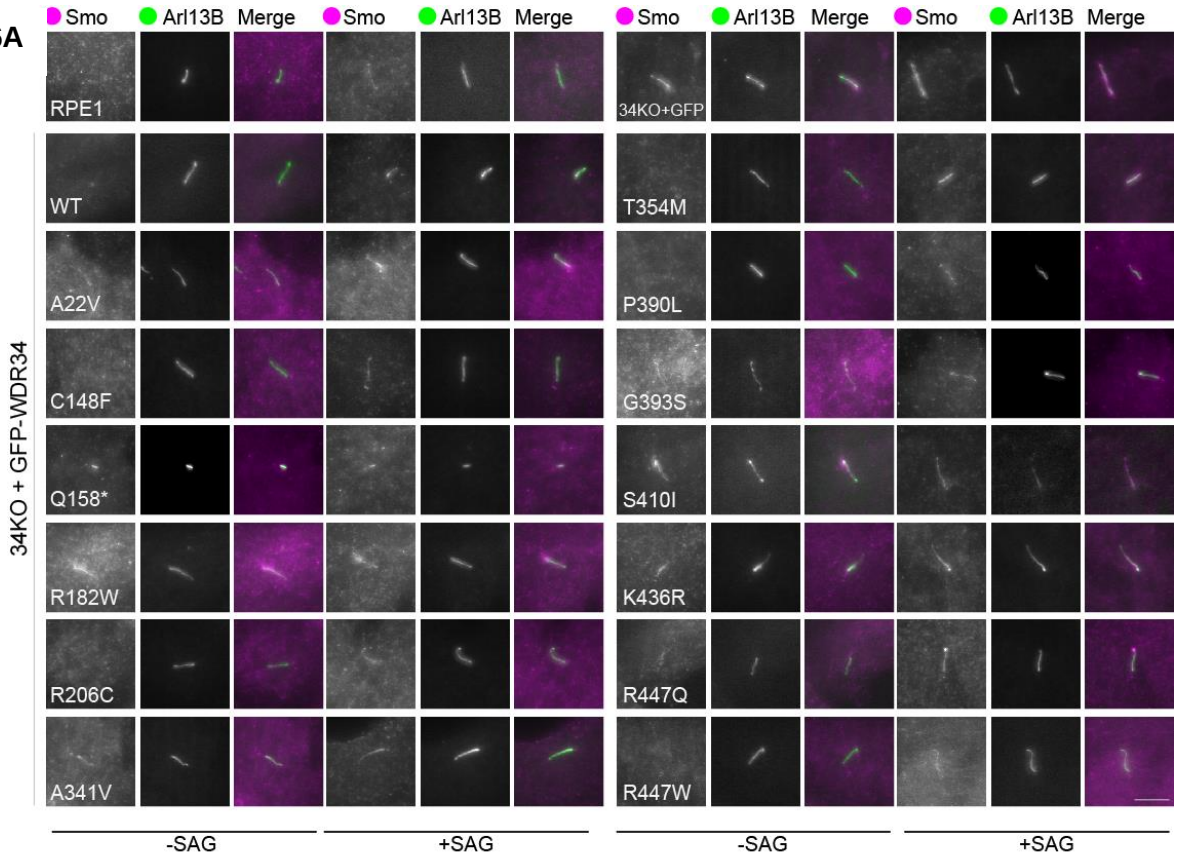

Fig 6B

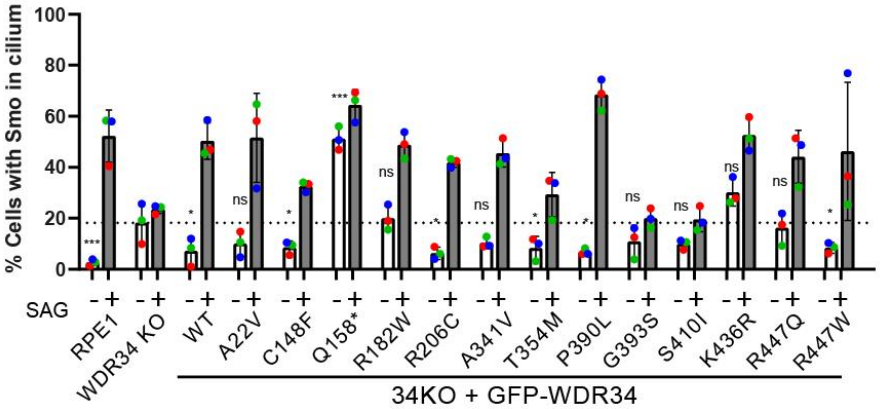

Figure 6 Analysis of Smo localization at steady state and following SAG stimulation. (A) Cells expressing WDR34 mutations were immunolabelled to detect Arl13b (green) and Smo (magenta). +/- SAG stimulation are shown. Scale bar = 5 µm. (B) Quantification of these data show the basal (open bars) and SAG-stimulated (gray bars) localization of Smo to cilia. Data show means and standard deviation, n=3 independent experiments. *P=<0.05 using Mann-Whitney test, comparing Smo levels under steady state only.

SAG stimulation led to Smo entry and accumulation in cilia in WT RPE1 cells (Fig. 6A, quantified in 6B). SAG treatment of cells expressing GFP resulted in only minor accumulation of Smo into the cilium. This contrasts with our previous work (Tsurumi et al., 2019) (Vuolo et al., 2018) using an alternative WDR34 KO cell line and likely results from either further time in culture or the stable expression of GFP in these cells. However, we could clearly define that cells expressing WDR34 WT and WDR34 mutants were responsive to SAG, shown by an increased proportion of cells with Smo in the axoneme. Interestingly, C148F, G393S, T354M and S410I mutations resulted in the least Smo accumulation and are also the mutations that led to weakened assembly of the core dynein-2 proteins. This suggests key roles for dynein-2 in the entry of Smo as well its exit from cilia.

Discussion

Skeletal ciliopathies caused by mutations in dynein-2 are well known for their poor correlation of genotypes and phenotypes (Huber and Cormier-Daire, 2012). Only limited work has been done on cells from these patients, in part hampered by limited availability of material. Our model provides for the opportunity to analyze the impact of many mutations in large numbers of cells. Many of the residues that are mutated are highly conserved through evolution (Supplementary Figure S1) and many are in regions likely to impact the folding or stability, either of WDR34 or of the entire dynein-2 complex (Supplementary Figure S2). We explored this using proteomics and then sought to correlate this with functional data from microscopy assays. Unfortunately, we were unable to define any clear common outcomes in relation to complex integrity, cilia length and number, IFT, or SAG responses (Supplementary Figure S4). Mutations in different regions of WDR34 can lead to a common phenotype, whereas those in close proximity can lead to a different set of cilia defects. Major impacts do depend, at least in part, on how effectively each WDR34 mutant is associated with other dynein-2 proteins. These data are summarized in Supplementary Figure S3. Since we were unable to cluster these phenotypes, we discuss each mutant individually.

A22V is at the N-terminal end of the protein. It has some effects on dynein-2 complex integrity, notably with regard to association with the WDR60-TCTEX module. Its expression effectively restores length and cilia number even above re-expression of WT GFP-WDR34 when expressed in WDR34 KO cells. It also fully restores the localization of RPGRIP1L and is most similar to the WT protein in terms of localization of IFT-A and IFT-B and Smo signalling . While it restores a normal SAG response, there remains a small but significant increase in basal Smo within cilia.

C148F shows defects in dynein-2 complex assembly or stability. It cannot restore the cilia length defect seen in WDR34 KO cells. It partially restores the steady-state distributions of RPGRIP1L and IFT-B. While C148F effectively rescues the basal exclusion of Smo from cilia, the SAG response is dampened, indicative of a defect in entry into cilia.

R182W results in an enhanced association with most dynein-2 subunits except for DYNLRB2. It restores cilia number even above re-expression of WT GFP-WDR34 and effectively restores cilia length, RPGRIP1L and IFT88 localization. It does not however act to remove the basal level of Smo from cilia seen in WDR34 KO cells. The SAG response remains robust indicating that the basal levels of Smo in cilia might underpin R182W related defects.

R206C shows a similar proteomic profile to R182W but shows other key differences. It restores the cilia length defect of WDR34 KO cells. It very effectively reverses the TZ defect shown with RPGRIP1L and IFT88 localization. A key difference to R182W is seen with Hh signalling where, while the SAG response also remains robust, R206C restores the basal exclusion of Smo from cilia.

A341V also shows a similar proteomic profile to R182W and R206C with enhanced association with DYNC2H1 and WDR60 with a significant reduction in association with DYNLRB1. Its profile is very similar to R182W in terms of cilia number and length, RPGRIP1L localization. A key difference is seen with IFT-B localization where IFT88 remains visible throughout the cilium. The Smo profile is very similar to that seen with WT GFP-WDR34.

T354M shows more dramatic changes in terms of the association with other dynein-2 subunits, notably DYNC2H1, WDR60, and DYNLRB2. It restores cilia length to normal, contrasting with shorter cilia observed in patient fibroblasts (Huber et al.,2013). RPGRIP1L is restored to the base of the cilium but IFT88 persists along the entire length. The basal exclusion of Smo from cilia is restored but the SAG response is somewhat reduced. This suggests a general reduction but not complete loss of dynein-2 activity.

Both A341 and T354 are close in proximity located on the fourth beta-propeller of WDR34 (Supplementary Figure S2). WDR34-A341V interaction with DYNCH1-LIC3 is increased 2-fold, whereas WDR34-T354M interaction with the other subcomplexes are drastically decreased. Hence, the IFT88 defect associated with the two mutations may be independent of dynein-2 assembly but depend on WDR34 folding. Both residues are located on opposite ends of consecutive beta-strands. Modelling of the mutations indicated that A341V leads to instability of the beta-propellor structure, with the mutant valine clashing with the first strand of the next propellor blade. Instead, T354 may form important hydrogen bonds important for maintaining structure stability, which are lost upon mutation into methionine.

P390L associates more strongly with the DYNC2H1 and WDR60 modules with some reduction in association with DYNLRB1. It restores cilia length and is highly effective in restoring the localization of RPGRIP1L to the base of the cilia. We see some very small defect in IFT88 localization but the SAG response mimics that of WT GFP-WDR34.

G393S shows the most dramatic changes in terms of association with other dynein-2 subunits with a reduction seen for all. It cannot restore normal cilia length, but is effective in terms of RPGRIP1L and IFT88 localization. The major defects seen with G393S are in Hh signalling with a near-complete failure to respond to SAG.

Similar to G393S, S410I fails to associate as effectively with other dynein-2 subunits and cannot restore cilia length. It restores RPGRIP1L to the base of the cilium, and IFT88 localization. It mirrors G393S with respect to absence of a robust SAG response. Together G393S and S410I link a failure of robust dynein-2 assembly to the ability of cells to respond to SAG. WDR34 G393S was identified in patients with anencephaly (Yin et al., 2020). Both here and in their study, the G393S mutation impairs Shh signalling .

K436R shows enhanced association with DYNC2H1 and to a lesser extent with WDR60. Cilia number and length, IFT88 and RPGRIP1L localization are restored to wild-type phenotypes but the basal levels of Smo in cilia are increased. In this regard it is highly similar to R182W in terms of impacts.

R447Q shows reduced association with most dynein-2 subunits. It rescues cilia number even above re-expression of WT GFP-WDR34 and retains the ability to restore cilia length, but not the localization of RPGRIP1L which remains extended into the TZ. This contrasts with shorter cilia observed in patient fibroblasts (Huber et al., 2013). However, IFT88 localization is restored indicating effective retrograde IFT. Notably, the basal levels of Smo within cilia remain high.

Surprisingly, R447W, unlike R447Q, only shows a loss of association with DYNLRB1.The percentage of ciliated cells is restored even above re-expression of WT GFP-WDR34 and cilia

length is restored as is the localization of RPGRIP1L and IFT88. The restoration of RPGRIP1L to the ciliary base contrasts with R447Q as does its ability to exclude Smo from the cilia in the basal state. The differences between the Q and W at this position suggest some critical differences. It seems unlikely that this would relate solely to folding of WDR34 but we note that R447W shows a reduced association with both DYNC2H1 and WDR60.

Overall, there are some common themes arising from this work.

Loss of light chain binding

We see more variation between the binding of dynein light chains, DYNLL1, DYNLL2 and DYNLRB1, to WDR34 mutants. Previous proteomic data showed that in the absence of WDR34, the other intermediate chain, WDR60, interacts less well with DYNLRB1 (Vuolo et al., 2018). Our data also showed that many WDR34 mutations, all located within a WD repeat domain, led to weak incorporation of the DYNLRB1 into the complex. Notably, the DYNLRB light chains lie in closest proximity to the WD repeat domains in the structure (Toropova et al., 2019). Mutations that did not affect the association of DYNLRB1 include A22V, which is located upstream of the DYNLRB1 binding site, R206V which is located between two WD repeat domains, and K436R in WD6. It may be that mutations within WD repeat domains commonly affect folding or stability of the beta propellor, transmitting to the region where DYNLRB1 binds. K436 is close in proximity to DYNC2H1 (Supplementary Figure S2), so although the residue is in a WD repeat domain, K436R may instead exert its mutant effect by affecting interaction with DYNC2H1.

Using deletion mutations Tsurumi et al. (2019) showed that residues 80-93 of WDR34 are required for its interaction with DYNLL2. Our data show that the interaction is also weakened by the A341V mutation, again showing that mutations downstream of the region, and further along in the WD domains are also able to affect interaction with proteins at the N-terminal end. This further supports a key role for WDR34 in the incorporation light chains to the dynein-2 complex (Hamada et al., 2018; Toropova et al., 2019; Tsurumi et al., 2019; Vuolo et al., 2020).

Impacts on IFT

In general, IFT140 localization remained consistent at the ciliary base in cells expressing GFP only or WDR34 missense mutations. IFT140 was enriched along the axoneme in cells expressing the Q158* truncation, similar to other models expressing short WDR34 N-terminal truncations (Tsurumi et al., 2019; Vuolo et al., 2018). IFT-A localization is affected in WDR60 KO cells (Vuolo et al., 2018) and DYNC2H1 mutant cells (Wu et al., 2017) suggesting that WDR34 may have no direct role in defining the steady-state localization of IFT-A. Localization of the IFT-B component IFT88 is abnormal in cells depleted of dynein-2 heavy chain, LIC3, WDR3, WDR60, or TCTEX1D2, or those retaining expression of short WDR34 fragments (Hamada et al., 2018; Kessler et al., 2015; Merrill et al., 2009; Taylor et al., 2015; Tsurumi et al., 2019; Vuolo et al., 2018). Expression of A341V and T354M mutations in WDR34 KO cells both failed to restore IFT88 to its normal distribution, suggesting that these residues have a more direct impact on retrograde IFT.

Impacts on the TZ

Localization of the transition zone protein RPGRIP1L is defective in WDR34 KO cells. Nearly all WDR34 mutations examined here restored this localization except for the C-terminal R447Q mutation. Surprisingly, R447Q, but not R447W leads to significant RPGRIP1L mis-localization, possibly due to differences in charge or steric changes impacting folding. WDR60 is also required for RPGRIP1L localization (Vuolo et al., 2018). Since WDR34-R447 does not lie in the vicinity of the interface with WDR60 (Toropova et al., 2019), it may be that the intermediate chains control the transition zone by different mechanisms.

Impacts on Hh signalling

Hh signalling is impaired in cells depleted of dynein-2 heavy chain, WDR60, LIC3 and those retaining expression of short WDR34 fragments (Hamada et al., 2018; Taylor et al., 2015; Tsurumi et al., 2019; Vuolo et al., 2018, Wu et al., 2015). The control of basal and SAG-stimulated levels of Smo are impaired in WDR34 KO cells and by different WDR34 mutations. G393S and S410I mutations reduce both basal Smo levels and SAG-induced translocation into cilia. A22V, R182W, A341V, K436R and R447Q mutations are unable to rescue the signalling impairment at basal conditions, but restore the response to SAG. C148F and T354M mutations can rescue basal Smo levels, but not Smo entry in response to SAG.

Perspective

Two of the mutations investigated here, T354M and R447W, were previously analysed in fibroblasts from patients with these mutations. Contrary to our results, both were found to result in shorter cilia (Huber et al., 2013). One reason for the inconsistency is that we are overexpressing the mutant proteins at much higher levels than normal, to be able to quantify large sample numbers which might restore some function. Furthermore, cilia formation differs between cell types such as fibroblasts and epithelial cells (Mazo et al., 2016).

As we were preparing this work for publication, Antony and colleagues (Antony et al., 2022) released a preprint that included analysis of two of the WDR34 mutants, R182W and G393S, included here using base editing of IMCD3 cells. This more precise approach to engineering mutants clearly has advantages in terms of engineering mutations into the endogenous locus and therefore avoiding limitations of overexpression. However, it comes with huge challenges regarding efficiency, complicated by the near-triploid state of IMCD3 cells. Their work defines more subtle, and sometimes contrasting phenotypes to ours. For both mutants, no significant changes to the ability of cells to form cilia, or in cilia length (Antony et al., 2022). Both mutants showed an increase in IFT88 at the ciliary tip, consistent with a defect in retrograde IFT. The data show a moderate increase in expression of GLI3 in both mutants as well as impaired Gli processing on SAG addition. These data are consistent with Shh signalling defects. In contrast, we find that overexpression of these mutants in a WDR34 KO background shows more clear defects with G393S showing the most significant changes in binding to other components of the dynein-2 complex and in Shh signalling . In contrast, our data show that R182W shows enhanced binding to dynein-2 subunits and can restore defects in ciliogenesis and IFT but not basal Smo accumulation in cilia. These differences are perhaps unsurprising given the very different model systems and in our case, we conclude that overexpression of R182W and G393S leads to more exaggerated outcomes than one would see with in locus base editing. Indeed, overexpression of G393S could even be acting as a dominant negative mutation. That said, expression levels of wild-type and mutant forms of WDR34 are broadly comparable in our experiments and we see robust functional rescue of many of the defects seen following KO of WDR34. Both approaches clearly have their merits. Base editing likely better reflects the clinical situation and gives a useful platform to screen for ways to alleviate phenotypes; our overexpression system provides some more insight into the biology of the system potentially leading to ways to achieve such interventions. Examples could include stabilizing assembly of the dynein-2 complex, controlling expression of mutant forms of WDR34, or targeting IFT or Hh signalling more selectively.

Patients with Jeune and short-rib polydactyly syndrome experience multi-organ abnormalities (Huber et al., 2013; Schmidts et al., 2013; You et al., 2017). Here, we have only studied a limited engineered cell system using epithelial cells. Cilia function is both cell-type and tissue-specific (Wheway et al., 2018). Of the mutations investigated in this study, polydactyly was reported in individuals with R182W, R206C and R447W mutations (Huber et al., 2013; Schmidts et al., 2013;

You et al., 2017). However, in this study, none of these mutations led to an increased baseline level of Smo in cilia. This might reflect cell-type specific differences.

All WDR34 mutations resulted in at least one cilia defect suggesting that these are major contributors to clinical phenotypes. Our results support the established roles of WDR34 in cilia extension, IFT-B maintenance, transition zone integrity, and Smo signalling . Notably, they also suggest that WDR34 does not have a single role within the dynein-2 complex and likely has multiple complex functions in assembly of IFT trains, activation of dynein-2, and retrograde IFT. Some patients carry compound mutations in other dynein-2 or IFT proteins which likely intensify cilia defects and the clinical phenotype. This is the case with A22V, P390L and R447Q. This highlights the need and challenge of understanding dynein-2 assembly, not only in the context of the holoenzyme, but also in terms of co-assembly with IFT-A, IFT-B, and kinesin-2.

Acknowledgements

We thank Anthony Roberts for helpful discussions throughout the project; members of the Stephens lab for continued discussion and help with this work; the Flow Cytometry and Wolfson Bioimaging Facilities for support and advice; Marc van der Kamp for advice on structural modelling and preparation of the figures. This work was funded by a JRPs-LEAD grant with UKRI-BBSRC from the Japan Society for the Promotion of Science (grant numbers JPJSJRP20181701 to K.N. and BB/S013024/1 to D.J.S).

Competing interests

D.J.S. is an Affiliate for bioRxiv. The authors declare no competing or financial interests.

Author contributions

Conceptualization: K.N., D.S.; Methodology: C.S., L.V., B.U., N.S., Y.K., K.H., D.S.; Validation: C.S., L.V., N.S., D.S.; Formal analysis: C.S., L.V., N.S., D.S.; Investigation: C.S., L.V., B.U., T.M., Y.K., N.S., K.H., D.S.; Data curation: C.S., D.S.; Writing - original draft: C.S., D.S.; Writing - review & editing: C.S., L.V., B.U., N.S., Y.K., K.N., D.S.; Visualization: C.S., D.S.; Supervision: K.N., L.V., N.S., D.S.; Project administration: K.N., D.S.; Funding acquisition: K.N., D.S.

Data access statement

Mass spectrometry data have been deposited to the ProteomeXchange Consortium via the PRIDE (Perez-Riverol et al., 2019) partner repository with the dataset identifier PXD032758.

Materials and Methods

Generation of WDR34 mutations

A plasmid encoding GFP-WDR34 was used as a template for site-directed mutagenesis performed by DC Biosciences Ltd (now Aruru Molecular Ltd, Dundee, UK). All were confirmed by Sanger sequencing. The Lenti-XTM HTX Packaging System (Clontech, Saint-Germain-en-Laye, France) was used with the appropriate plasmid (generated by DC Bioscience) to generate lentiviral particles in HEK293T cells. The resultant viral supernatant was used to transduce RPE1 cells, which were then cultured in complete medium with the addition of 5 µg/ml puromycin. Cells were sorted by fluorescence activated cell sorting using the University of Bristol Flow Cytometry Facility.

Cell culture

RPE1 and HEK293T cells were obtained from ATCC. WDR34 KO (WDR34 KO-1-5), derived by genome engineering from RPE1 cells are described in (Tsurumi et al., 2019). HEK293T cells were cultured in in Dulbecco's modified Eagle's medium (DMEM) supplemented with 10% FBS, whereas RPE1 cells were cultured in DMEM/F12 supplemented with 10% FBS. For ciliogenesis, cells were washed in PBS followed by serum starvation, by incubation in with media without FBS, for 24 h. All cells were grown at 37ºC and 5% CO2.

Five of the WDR34 KO cell lines expressing GFP proteins were contaminated with mycoplasma. They were treated with plasmocin (Invivogen) for two weeks as per the manufacturer's guidelines. All cells were from then on grown in the absence of plasmocin and verified independently to be free from mycoplasma contamination (MWG Eurofins).

To induce Hh signalling , cells were seeded and the next day treated with 200 nM SAG, together with serum starvation for 24 hour before harvesting of cells.

Antibodies

Antibodies used were as follows. Acetylated tubulin (Sigma-Aldrich, Cat# T6793, RRID:AB_477585, used 1:1000 for immunofluorescence); Arl13b (Proteintech, Cat# 17711–1-AP, RRID:AB_2060867, 1:1000 for immunofluorescence); Arl13b (Proteintech, Cat# 66739-1-Ig, RRID:AB_2882088, 1:1000 for immunofluorescence); GAPDH (Proteintech, Cat# 60004-1-Ig, RRID:AB_2107436, 1:5000 for immunoblotting); GFP (BioLegend, Cat# 902601, RRID:AB_2565021, 1:5000 for immunoblotting); IFT88 (Proteintech, Cat# 13967-1-AP, RRID:AB_2121979, 1:300 for immunofluorescence); IFT140 (Proteintech, 17460-1-AP, RRID:AB_2295648, 1:100 for immunofluorescence); RPGRIP1L (Proteintech, Cat# 55160–1-AP, RRID:AB_10860269, 1:200 for immunofluorescence); Smoothened, Santa Cruz Biotechnology, Cat# sc-166685, RRID:AB_2239686, 1:100 for immunofluorescence).

Immunofluorescence

Uncoated #1.5 glass coverslips were used for the culturing of cells for immunofluorescence microscopy. Depending on the antibody to be used, cells were fixed with −20°C methanol for 5 min, or with 4% PFA for 10 mins before extraction using 0.1% triton/PBS. Cells were blocked in 3% bovine serum albumin (BSA)/PBS for 30 min, followed by incubation in primary antibody solution in 3% BSA/PBS for 1 h, then in secondary antibody and DAPI (0.5 µg/ml) solution in 3% BSA/PBS for 1 h, all with PBS washes in between. Coverslips were mounted on microscope slides with Mowiol 4-88 mounting medium.

Cells were imaged using an Olympus IX- 71 widefield microscope with a 63x objective, and excitation and emission filter sets (Semrock, Rochester, NY) controlled by Volocity software (version 4.3, Perkin-Elmer, Seer Green, UK). Images were processed using FIJI (Schindelin et al., 2012).

Immunoblotting

Cells were lysed in RIPA buffer (50 mM Tris-HCl pH 7.5, 150 mM NaCl, 1% Triton X-100, 1% sodium deoxycholate, 0.1% SDS, 1 mM EDTA and protease inhibitors (539137, Millipore)). LDS buffer was added to clarified lysates. Protein samples were separated on 4-12% Bis-Tris gels and transferred onto nitrocellulose membranes by wet transfer. Membranes were blocked with 5% milk/PBST for 1 h, incubated in blocking solution with primary antibodies overnight, then incubated with HRP-conjugated secondary antibodies for one hour. Blots were developed by chemiluminescence.

Immunoprecipitation

Cells ready for harvest were first incubated with 1 mM DSP for 30 min on ice to cross-link proteins. The reaction was quenched by the addition of 500 mM Tris-HCl pH 7.5 for 15 min. Cells were then washed with PBS and scraped off the plate in lysis buffer (10 mM Tris pH 7.4, 150 mM NaCl, 0.5 mM EDTA, 0.5% IGEPAL and protease inhibitors) followed by incubation on ice for 30 min. Clarified lysates were retrieved by centrifugation and incubated for 3 h on a rotating wheel at 4ºC with 20 µl GFP-Trap beads. Beads were washed three times in washing buffer (10 mM Tris pH 7.4, 150 mM NaCl, 0.5 mM EDTA). Beads for proteomics analysis were resuspended in minimal volume of wash buffer.

Proteomic analysis

Proteomic analysis including Nano LC mass spectrometry and primary data analysis was done as described in Vuolo et al (2018).

References

Antony, D., Güleç, E. Y., Bakey, Z., Schüle, I., Kim, G.-J., Skatulla, I., Brunner, H. G., Arnold, S. J. and Schmidts, M. (2022). Base editing derived models of human WDR34 and WDR60 disease alleles replicate retrograde IFT and hedgehog signalling defects and suggest disturbed Golgi protein transport. *bioRxiv*, 2022.03.14.483768.

Asante, D., Stevenson, N. L. and Stephens, D. J. (2014). Subunit composition of the human cytoplasmic dynein-2 complex. *Journal of cell science* **127**, 4774-87.

De-Castro, A. R. G., Rodrigues, D. R. M., De-Castro, M. J. G., Vieira, N., Vieira, C., Carvalho, A. X., Gassmann, R., Abreu, C. M. C. and Dantas, T. J. (2022). WDR60-mediated dynein-2 loading into cilia powers retrograde IFT and transition zone crossing. *Journal of Cell Biology* **221**.

Funabashi, T., Katoh, Y., Okazaki, M., Sugawa, M. and Nakayama, K. (2018). Interaction of heterotrimeric kinesin-II with IFT-B-connecting tetramer is crucial for ciliogenesis. *Journal of Cell Biology* **217**, 2867-2876.

Gilula, N. B. and Satir, P. (1972). The ciliary necklace. A ciliary membrane specialization. *Journal of Cell Biology* **53**, 494-509.

Goetz, S. C. and Anderson, K. V. (2010). The primary cilium: a signalling centre during vertebrate development. *Nature reviews. Genetics* **11**, 331-44.

Grissom, P. M., Vaisberg, E. A. and McIntosh, J. R. (2002). Identification of a novel light intermediate chain (D2LIC) for mammalian cytoplasmic dynein 2. *Molecular Biology of the Cell* **13**, 817-29.

Hamada, Y., Tsurumi, Y., Nozaki, S., Katoh, Y. and Nakayama, K. (2018). Interaction of WDR60 intermediate chain with TCTEX1D2 light chain of the dynein-2 complex is crucial for ciliary protein trafficking. *Molecular biology of the cell* **29**, 1628-1639.

Hirano, T., Katoh, Y. and Nakayama, K. (2017). Intraflagellar transport-A complex mediates ciliary entry and retrograde trafficking of ciliary G protein-coupled receptors. *Molecular biology of the cell* **28**, 429-439.

Hou, Y., Pazour, G. J. and Witman, G. B. (2004). A dynein light intermediate chain, D1bLIC, is required for retrograde intraflagellar transport. *Molecular biology of the cell* **15**, 4382-94.

Huber, C. and Cormier-Daire, V. (2012). Ciliary disorder of the skeleton. *Am J Med Genet C Semin Med Genet* **160C**, 165-74.

Huber, C., Wu, S., Kim, A. S., Sigaudy, S., Sarukhanov, A., Serre, V., Baujat, G., Le Quan Sang, K. H., Rimoin, D. L., Cohn, D. H. et al. (2013). WDR34 mutations that cause short-rib polydactyly syndrome type III/severe asphyxiating thoracic dysplasia reveal a role for the NF-kappaB pathway in cilia. *Am J Hum Genet* **93**, 926-31.

Jensen, V. L., Lambacher, N. J., Li, C., Mohan, S., Williams, C. L., Inglis, P. N., Yoder, B. K., Blacque, O. E. and Leroux, M. R. (2018). Role for intraflagellar transport in building a functional transition zone. *EMBO Rep* **19**.

Jordan, M. A., Diener, D. R., Stepanek, L. and Pigino, G. (2018). The cryo-EM structure of intraflagellar transport trains reveals how dynein is inactivated to ensure unidirectional anterograde movement in cilia. *Nature Cell Biology* **20**, 1250-1255.

Kessler, K., Wunderlich, I., Uebe, S., Falk, N. S., Giessl, A., Brandstatter, J. H., Popp, B., Klinger, P., Ekici, A. B., Sticht, H. et al. (2015). DYNC2LI1 mutations broaden the clinical spectrum of dynein-2 defects. *Scientific reports* **5**, 11649.

Kozminski, K. G., Johnson, K. A., Forscher, P. and Rosenbaum, J. L. (1993). A motility in the eukaryotic flagellum unrelated to flagellar beating. *Proc Natl Acad Sci U S A* **90**, 5519-23.

Mazo, G., Soplop, N., Wang, W. J., Uryu, K. and Tsou, M. F. (2016). Spatial Control of Primary Ciliogenesis by Subdistal Appendages Alters Sensation-Associated Properties of Cilia. *Developmental Cell* **39**, 424-437.

Merrill, A. E., Merriman, B., Farrington-Rock, C., Camacho, N., Sebald, E. T., Funari, V. A., Schibler, M. J., Firestein, M. H., Cohn, Z. A., Priore, M. A. et al. (2009). Ciliary Abnormalities Due to Defects in the Retrograde Transport Protein DYNC2H1 in Short-Rib Polydactyly Syndrome. *American Journal of Human Genetics* **84**, 542-549.

Nievergelt, A. P., Zykov, I., Diener, D., Buchholz, T.-O., Delling, M., Diez, S., Jug, F., Štěpánek, L. and Pigino, G. (2021). Intraflagellar transport trains can turn around without the ciliary tip complex. *bioRxiv*, 2021.03.19.436138.

Park, K. and Leroux, M. R. (2022). IFT trains overcome an NPHP module barrier at the transition zone. *Journal of Cell Biology* **221**.

Patel-King, R. S., Gilberti, R. M., Hom, E. F. and King, S. M. (2013). WD60/FAP163 is a dynein intermediate chain required for retrograde intraflagellar transport in cilia. *Molecular biology of the cell* **24**, 2668-77.

Pazour, G. J., Dickert, B. L. and Witman, G. B. (1999). The DHC1b (DHC2) isoform of cytoplasmic dynein is required for flagellar assembly. *Journal of Cell Biology* **144**, 473-81.

Pazour, G. J., Wilkerson, C. G. and Witman, G. B. (1998). A dynein light chain is essential for the retrograde particle movement of intraflagellar transport (IFT). *Journal of Cell Biology* **141**, 979-92.

Pigino, G. (2021). Intraflagellar transport. *Current Biology* **31**, R530-R536.

Porter, M. E., Bower, R., Knott, J. A., Byrd, P. and Dentler, W. (1999). Cytoplasmic dynein heavy chain 1b is required for flagellar assembly in Chlamydomonas. *Molecular biology of the cell* **10**, 693-712.

Reiter, J. F. and Leroux, M. R. (2017). Genes and molecular pathways underpinning ciliopathies. *Nat Rev Mol Cell Biol* **18**, 533-547.

Rompolas, P., Pedersen, L. B., Patel-King, R. S. and King, S. M. (2007). Chlamydomonas FAP133 is a dynein intermediate chain associated with the retrograde intraflagellar transport motor. *Journal of Cell Science* **120**, 3653-65.

Schindelin, J., Arganda-Carreras, I., Frise, E., Kaynig, V., Longair, M., Pietzsch, T., Preibisch, S., Rueden, C., Saalfeld, S., Schmid, B. et al. (2012). Fiji: an open-source platform for biological-image analysis. *Nature Methods* **9**, 676-82.

Schmidts, M., Vodopiutz, J., Christou-Savina, S., Cortes, C. R., McInerney-Leo, A. M., Emes, R. D., Arts, H. H., Tuysuz, B., D'Silva, J., Leo, P. J. et al. (2013). Mutations in the gene encoding IFT dynein complex component WDR34 cause Jeune asphyxiating thoracic dystrophy. *Am J Hum Genet* **93**, 932-44.

Signor, D., Wedaman, K. P., Orozco, J. T., Dwyer, N. D., Bargmann, C. I., Rose, L. S. and Scholey, J. M. (1999). Role of a class DHC1b dynein in retrograde transport of IFT motors

and IFT raft particles along cilia, but not dendrites, in chemosensory neurons of living Caenorhabditis elegans. *Journal of Cell Biology* **147**, 519-30.

Stepanek, L. and Pigino, G. (2016). Microtubule doublets are double-track railways for intraflagellar transport trains. *Science* **352**, 721-4.

Takahara, M., Kunii, M., Nakamura, K., Harada, A., Hirano, T., Katoh, Y. and Nakayama, K. (2019). C11ORF74 interacts with the IFT-A complex and participates in ciliary BBSome localization. *Journal of Biochemistry* **165**, 257-267.

Taylor, S. P., Dantas, T. J., Duran, I., Wu, S., Lachman, R. S., University of Washington Center for Mendelian Genomics, C., Nelson, S. F., Cohn, D. H., Vallee, R. B. and Krakow, D. (2015). Mutations in DYNC2LI1 disrupt cilia function and cause short rib polydactyly syndrome. *Nature communications* **6**, 7092.

Toropova, K., Mladenov, M. and Roberts, A. J. (2017). Intraflagellar transport dynein is autoinhibited by trapping of its mechanical and track-binding elements. *Nat Struct Mol Biol* **24**, 461-468.

Toropova, K., Zalyte, R., Mukhopadhyay, A. G., Mladenov, M., Carter, A. P. and Roberts, A. J. (2019). Structure of the dynein-2 complex and its assembly with intraflagellar transport trains. *Nat Struct Mol Biol* **26**, 823-829.

Tsurumi, Y., Hamada, Y., Katoh, Y. and Nakayama, K. (2019). Interactions of the dynein-2 intermediate chain WDR34 with the light chains are required for ciliary retrograde protein trafficking. *Molecular biology of the cell* **30**, 658-670.

Vuolo, L., Stevenson, N. L., Heesom, K. J. and Stephens, D. J. (2018). Dynein-2 intermediate chains play crucial but distinct roles in primary cilia formation and function. *eLife* **7**.

Vuolo, L., Stevenson, N. L., Mukhopadhyay, A. G., Roberts, A. J. and Stephens, D. J. (2020). Cytoplasmic dynein-2 at a glance. *Journal of cell science* **133**.

Webb, S., Mukhopadhyay, A. G. and Roberts, A. J. (2020). Intraflagellar transport trains and motors: Insights from structure. *Semin Cell Dev Biol* **107**, 82-90.

Wheway, G., Nazlamova, L. and Hancock, J. T. (2018). Signalling through the Primary Cilium. *Front Cell Dev Biol* **6**, 8.

Wu, C., Li, J., Peterson, A., Tao, K. and Wang, B. (2017). Loss of dynein-2 intermediate chain Wdr34 results in defects in retrograde ciliary protein trafficking and Hedgehog signalling in the mouse. *Human molecular genetics* **26**, 2386-2397.

Yin, H., Peng, R., Chen, Z., Wang, H., Zhang, T. and Zheng, Y. (2020). WDR34 mutation from anencephaly patients impaired both SHH and PCP signalling pathways. *J Hum Genet* **65**, 985-993.

You, S. H., Lee, Y. S., Lee, C. P., Lin, C. P., Lin, C. Y., Tsai, C. L., Chang, Y. L., Cheng, P. J., Wang, T. H. and Chang, S. D. (2017). Identification of a c.544C>T mutation in WDR34 as a deleterious recessive allele of short rib-polydactyly syndrome. *Taiwanese journal of obstetrics & gynecology* **56**, 857-862.